RECENT DEVELOPMENTS ON THE STANFORD 500 MEV ELECTRON STORAGE RINGS *

Bernard Gittelman †
Stanford University
Stanford, California

SUMMARY

Large angle electron scattering has been detected on the Stanford storage rings. The operation of the rings is now adequate to proceed with the proposed test of quantum electrodynamics. A discussion of the event rate and possible limitations on this rate is given.

The Princeton-Stanford storage ring group, consisting of B. Richter, W. C. Barber, G. K. O'Neill and myself, have been working at Stanford for the past six years to do electron-electron scattering at a center of mass energy of 1 BeV by making collisions between two stored electron beams. The design of the storage rings has been described in our proposal[1]. Figure 1 is the schematic layout of the rings. Electrons from the Stanford Mark III accelerator are injected, on alternate beam pulses into each ring. The linac is operated at 30 cps and after a time of the order of a minute a stacked beam of 50 to 100 ma is built up in each ring. In the straight section common to the rings the circulating beam bunches can be made to pass through each other. Most of the work has been carried out at our injection energy of 300 MeV.

The problems associated with injection and storage lifetime have been under control for more than a year. The past year we have been studying the beam instabilities that develop when the beams pass through each other. Considerable progress has been made toward understanding the limitations imposed by instabilities and learning to live within these limitations. Recently we have observed electron-electron scattering at a rate sufficiently high to proceed with our proposed experiment.

Figure 2b is a side view of the interaction straight section showing the spark chamber detector. If a scattering occurs the electrons come out with equal but opposite momentum. For scattering angles in the range $35 < \theta < 90$ and for a rather narrow range of 26° in azimuth, the scattered particles pass through the spark chambers and trigger counters 5, 6, 7, 8, 9 and 10. Counters 1, 2, 3 and 4 provide cosmic ray vetoing. A veto signal is produced whenever any two of these counters are triggered. There are six inches of lead between the spark chambers and veto counters to absorb the upward going electrons. Less than 1% of these will produce a cosmic ray veto signal. The spark chamber is normally triggered on $(5 + 6 + 7 + 8 + 9 + 10) + \overline{(\text{any pair of } 1, 2, 3, 4)}$.

Data on electron-electron scattering was accumulated during six consecutive 12-hour shifts on the Mark III accelerator. A standard run consisted of filling the rings to 30 to 50 ma, turning off the linac and installing the spark chamber camera, switching the various beam steering magnets from their injection setting to their interacting setting, and turning on the counters and counting for 1500 seconds. We recorded spark chamber frame number and beam currents every 500 seconds. The currents at which we started counting varied from ≃ 20 ma in the early runs to ≃ 35 ma in the late runs. There were a total of 70 runs made with the beams interacting in such a way as to give electron-electron scattering events in the spark chambers. These runs were separated by a single series of 22 runs in which the RF cavities were dephased by 4 nanoseconds so that the bunched beams passed through each other at the end of the straight section, a place in which electron-electron scattering events would not be recorded in the spark chambers.

In the "phased" situation, a total of 10^4 spark chamber pictures were taken. Figures 2 through 6 are sample spark chamber pictures. In each, (a) is the picture as it appears on the film and (b) is the event reconstructed on a scale drawing of the straight section and detector. Figures 2 and 3 are typical collinear events. Figure 4 is a non-collinear event which is what one should get from an electron spill. A large fraction of the pictures look like this. Figure 5 is a rare picture. We interpreted this as probably an electron-electron scattering which occurred outside of the usable region of the straight section. The downward directed electron passes through the vacuum chamber wall at the base of the dome and a delta ray was emitted. The upward going electron produced a knock-on in the counter or steel dome just below the spark chamber. Figure 6 is typical of 5 or 10% of the pictures.

The films were scanned for collinear tracks (within 5°) in the upper and lower chambers. For those events, the coordinates of the intersection of the straight line and the median plane of the vacuum chamber were recorded along with the two angles defined by the projections of the tracks. Figures 7 and 8 are scatter plots of all the collinear events from the phased runs and dephased runs, respectively. Figure 9 is the longitudinal distribution summed over radial positions and Figure 10 is the radial distribution for the phased runs. I should mention that the spark chamber has a clear view of events occurring only within 2 inches of the center of the straight section along the direction of beam motion. Limiting ourselves to ± 2 inches along beam line and ± 0.5 inches transverse to beam line, we ended up with 77 events.

The 22 runs with beams dephased have a distribution consistent with what is seen outside of the region ± 0.5 inches transverse to the beam in the phased runs. Their distribution and rate are also consistent with measurements of cosmic rays leaking through the veto counters. The dephased runs tell us that 4 ± 2 of the 77 events are cosmic rays.

The rate at which we should observe electron scattering is given by:

$$R = K_N N_1 N_2 = K_I I_1 I_2$$

where N_1, N_2 are the number particles in each ring. I_1, I_2 are the currents associated with that number of particles. If the beams are stable and optimally aligned, then K is independent of the beam currents and is given by:

$$K_N = \frac{f}{2wh}\left(\frac{2d\nu}{\sqrt{2}\,\ell}\right)\left(\int \frac{d\sigma}{d\Omega}\, d\Omega\right)\epsilon$$

$$K_I = (2.5 \times 10^8)^2\, K_N \quad \text{for currents in milliamps}$$

Here

f is the RF frequency, 25×10^6 sec^{-1}

$\int \frac{d\sigma}{d\Omega}\, d\Omega$ is the Møller cross section^2 integrated over the angles subtended by the detector, 7.2×10^{-31} cm^2.

d is the interaction length observed, 10 cm.

ℓ is an effective beam length,

$$\ell = \frac{1}{\sqrt{2}}\sqrt{\ell_1^2 + \ell_2^2} = 60 \text{ cm}$$

w is an effective beam width,

$$w = \frac{\xi}{\sqrt{2}}\sqrt{w_1^2 + w_2^2} = 0.3 \text{ cm}$$

h is an effective beam height,

$$h = \frac{\xi}{\sqrt{2}}\sqrt{h_1^2 + h_2^2} = 0.08 \text{ cm}$$

$$\xi = \left(\frac{\pi}{4 \log 2}\right)^{1/2} \simeq 1.06$$

$$\nu = \frac{\sqrt{2}\,\ell}{2d}\,\text{erf}\left[\frac{d(2 \log 2)^{1/2}}{\ell}\right] =$$

$$\frac{1}{\xi} \text{ for } d \ll \ell$$

We have assumed the beams have gaussian distributions in length, width, and height. $\ell_{\frac{1}{2}}$, $w_{\frac{1}{2}}$, and $h_{\frac{1}{2}}$ are the full width at half the maximum intensity.

ϵ is the efficiency of the six-fold trigger system, 0.80. Putting these numbers together gives:

$$\frac{R}{I_1 I_2} = K_I = 4.4 \times 10^{-6}\ \frac{\text{events}}{\text{ma}^2\ \text{sec}}$$

To discuss storage ring capabilities, one prefers a number which is independent of physical scattering process and detector. The luminosity, L, is the interaction rate per unit cross section.

$$L = \frac{R}{\left(\frac{2d\nu}{\sqrt{2}\,\ell}\right)\left(\int \frac{d\sigma}{d\Omega}\, d\Omega\right)\epsilon}$$

$$\frac{L}{I_1 I_2} = 3.2 \times 10^{25}\ \text{sec}^{-1}\ \text{cm}^{-2}\ \text{ma}^{-2}$$

This calculation of the counting rate implicitly assumes that the beam length, ℓ, width, w, and height, h, are fixed and that the beams are diffuse within those dimensions. As an instability developed one might expect K to decrease.

Table I is a summary of the number of real events at each beam current level. From the entries under $R/I_1 I_2$ we see there is no significant decrease in K up to currents of 28 to 40 ma per ring. The average measured rate per ma^2 was 2.3×10^{-6}. Although this differs from the calculated rate by a factor 2, I consider the agreement very good in view of the uncertainties in a number of the experimental quantities.

As many people know, we have been complaining this past year that storage rings provide vivid demonstrations of relativistic space charge instabilities in circular accelerators. The obvious question to be asked is what have we done to cure our instability problems. At the moment we are in the position of having found a sufficient set of conditions to operate the rings. We do not know if all of them are necessary. I should mention that many of the fancy gadgets that were added to the rings since our original proposal were motivated by discussions with A. Sessler, J. Laslett, E. Courant and, especially, D. Ritson.

The present picture of the instabilities is still very cloudy. Experimentally, we believe we have seen several different types of instabilities. Theoretically, two of the instability models that have been investigated bear some resemblance to the experimental situation and it is believed that either or both may be limiting our achievable luminosity.

The first I shall refer to as the single particle interacting with a potential (SPIP) model. One assumes Beam 2 is stiff and presents a fixed force field over a limited region of space to individual particles in Beam 1. One calculates what happens to the particle orbit and

finds a limiting strength of the force field for which the particle from Beam 1 fails to pass through the Beam 2 bunch. Amman and Ritson[3] have given an analytical solution to this problem considering only vertical motion and a linear force field over beam dimensions. Recently, E. Courant[4] has extended this work to a more realistic force field and two dimensional betatron motion by calculating particle orbits on a computer. The force field strength is most conveniently expressed in terms of the shift in betatron frequency or Q value it induces in the particle orbit. Amman and Ritson suggested that one could expect stability up to the point at which the individual particle betatron frequency is shifted by an amount large enough to put the particle on a proper machine resonance. Calling this frequency shift ΔQ, this would mean a $\Delta Q \lesssim 0.2$ for our machine. The calculation of E. Courant reduced this number to 0.05 to 0.1 for an allowable interaction strength.

For example, if Beam 2 consists of N_2 particles distributed uniformly inside a width, w, and height, h (we assume $h \ll w$), then the change in vertical Q value of a particle in Beam 1 is given by:

$$\Delta Q_1 = \frac{N_2}{wh} \frac{r_e R_M}{\gamma Q_1}$$

where r_e is the classical electron radius, R_M is the mean machine radius, and γ is the relativistic energy to mass ratio. Using $\Delta Q = 0.1$ we get a maximum value for

$$\frac{N}{wh} = \frac{\Delta Q \gamma Q}{r_e R_M} = \frac{0.1(600)(0.9)}{2.8 \times 10^{-13} \times 200} \simeq 10^{12} \text{ cm}^{-2}$$

[Note: this number is the maximum target thickness of a storage ring. Then Nf is the incident flux and the interaction rate per unit cross section, L, is given by:

$$L \simeq \frac{N}{wh}(Nf) = \frac{N}{wh}^2 f(wh) \;]$$

At this point one concludes that maximum luminosity is achieved by making (wh) as large as possible provided one can increase N so that $(\frac{N}{wh})$ is at its largest permissable value.

The second type of instability I will refer to as the coupled beam-resistive wall vertical instability (CBRW)[5]. The ideas associated with this were a direct outgrowth of the paper of Laslett, Neil and Sessler[6] on single beam resistive wall instabilities. Here one considers, besides the interaction of the single beam with the walls of the vacuum chamber, the coupling between the two beam bunches. In our latest version one obtains an instability threshold of the form:

$$\left[\frac{N_1 r_e R_M}{w_1 h_1 \gamma Q_1}\right]\left[\frac{N_2 r_e R_M}{w_2 h_2 \gamma Q_2}\right] \frac{1}{\delta Q_1 (Q_1 - Q_2)} \simeq 1$$

Here we are assuming Beam 1 goes unstable. Then δQ_1 is the spread of vertical betatron Q values about Q_1 of the individual particles in Beam 1. $(Q_1 - Q_2)$ is the difference in the Q values and we assume $(Q_1 - Q_2) \gg \delta Q_2$ [if this condition is not met then $(Q_1 - Q_2)$ gets replaced by $\left\{(Q_1 - Q_2)^2 + (\delta Q_2)^2\right\}^{1/2}$]. One expects δQ is of the order of but less than ΔQ, the frequency shift discussed in the SPIP model, since the interaction between the two beams is the strongest non-linear element in the system.

If $\delta Q = \Delta Q$ then the two instabilities appear at the same current level for $Q_1 = Q_2$, otherwise CBRW dominates for Q_1 sufficiently close to Q_2. D. Ritson[7] has estimated $\delta Q \simeq \frac{1}{3} \Delta Q$. In this case one must split the Q's by an amount equal to $3\Delta Q_{max}$ in order to be able to operate stably at that ΔQ_{max}.

To summarize, the proper line of experimental approach is to make the beam cross section (wh) as large as possible, make $(Q_1 - Q_2)$ as large as possible and then choose beam currents that will not violate either of the above instability limits. Using a quadrupole magnet on each ring we split the Q's so that $Q_1 - Q_2 = 0.05$. Using a rotated quadrupole on each ring we coupled radial motion into vertical motion, thereby increasing the beam height from ~0.1 mm to ~ 0.8 mm. Assuming a ΔQ_{max} limitation of $1/3 \times 0.05 \simeq 0.02$, we concluded a safe beam current is 20 ma. From this one gets a maximum luminosity of 1.25×10^{28}. Actually we ran about 20% of the time at currents above the 20 ma level, and as I mentioned there was no significant decrease in the luminosity per ma^2. Considering the uncertainties involved, it is not significant that we did not see a fall off in the interaction rate. Furthermore, at our highest beam currents (>30 ma), we already see pieces of the beam get lost in a discontinuous manner.

Most of the ideas presented here on instabilities are tentative. Experimentally, all we know is that increasing the beam height and splitting the Q values has led to a reasonable interaction rate. Although we do not yet have conclusive evidence that both of these steps are necessary, we suspect so. A conclusive test which we shall make is to study the maximum obtainable luminosity as a function of $(Q_1 - Q_2)$. However, our personal prejudices require that we first do the electron-electron scattering experiment.

References

1. W. C. Barber, B. Richter, W. K. H. Panofsky, G. K. O'Neill and B. Gittelman, "An Experiment on the Limits of Quantum Electrodynamics" Hansen Laboratory Report, HEPL 170 (June 1959)

2. J. M. Jauch and F. Rohrlich, The Theory of Photons and Electrons, Addison Wesley Publishing Co., Inc., Reading, Mass., 1955, 2nd ed., Chap. 12, p. 254.

3. F. Amman and D. Ritson, "Space Charge Effects in e^-e^- and e^+e^- Colliding or Crossing Beam Rings", Frascati Internal Report.

4. E. Courant, (Private communication, results to be presented at this conference).

5. A. Sessler did the original work on this last summer. The author is indebted to E. Courant and D. Ritson for some of the additions and reinterpretations.

6. L. J. Laslett, V. K. Neil, A. M. Sessler, "Transverse Resistive Instabilities of Intense Coasting Beams in Particle Accelerators", Lawrence Radiation Laboratory Report, UCRL-11090, (Oct. 25, 1963).

7. D. Ritson, (Private communication).

Footnotes

* Work supported in part by the Office of Naval Research contract Nonr 225 (67).

† On leave from the Department of Physics, Princeton University.

TABLE I

SUMMARY OF RESULTS OF PHASED RUNS-DEPENDENCE ON CURRENT LEVEL

Range of $I_1 I_2$ $(ma)^2$		50-100	100-200	200-400	400-800	800-1600	Total
Number of events, N		1	16	33	21	5	77
$\sum_{\text{Runs}} \int_{(I_1I_2)_{min}}^{(I_1I_2)_{max}} I_1 I_2 dt$ $(\times 10^5$ ma^2 sec)		3.8	52	134	89	25	338
$\int_{(I_1I_2)_{min}}^{(I_1I_2)_{max}} I_1 I_2 dt$ $(\times 10^5$ ma^2 sec)	I	0.76	1.29	2.11	2.50	--	
	II	--	1.47	2.47	3.66	4.07	
Half Life, τ (sec)	I	900	900	750	450	--	
	II	--	1020	880	650	360	
Actual Running Time, T $(\times 10^3$ sec)		4.5	36	48	16	2.2	107
$\frac{R}{I_1 I_2} = \frac{N}{\Sigma_{\text{runs}} \int I_1 I_2 dt}$ $(\times 10^{-6}$ ma^{-2} sec^{-1}		2.6 ± 2.6	3.1 ± 0.78	2.46 ± 0.45	2.36 ± 0.50	2.0 ± 0.9	2.3 ± 0.26
$\left[\frac{L}{I_1 I_2}\right]$ $(\times 10^{25}$ cm^{-2} ma^{-2} sec^{-1})		1.9 ± 1.9	2.3 ± 0.57	1.8 ± 0.32	1.7 ± 0.37	1.5 ± 0.62	1.7 ± 0.19
Luminosity, L $(\times 10^{27}$ cm^{-2} sec^{-1})		1.6 ± 1.6	3.2 ± 0.82	5.0 ± 0.91	9.8 ± 2.0	17 ± 7	

NOTES FOR TABLE I

1. N is the number of events (scattering angle between 35° and 90°) occurring at current level, I_1I_2, which lies in the range $(I_1I_2)_{min}$ and $(I_1I_2)_{max} = 2(I_1I_2)_{min}$.

2. Actual running time was computed from:

$$T = \frac{\tau \sum_{runs} \int_{(I_1I_2)_{max}}^{(I_1I_2)_{min}} I_1I_2 dt}{\int_{(I_1I_2)_{max}}^{(I_1I_2)_{min}} I_1I_2 dt}$$

3. Luminosity per ma^2 was computed from:

$$\left[\frac{L}{I_1I_2}\right] = \frac{R}{I_1I_2} \frac{1}{\left(\frac{2d}{\sqrt{2}\,\ell}\right)\left(\int \frac{d\sigma}{d\Omega}\, d\Omega\right) \epsilon} = \frac{R}{I_1I_2} (0.74 \times 10^{31})$$

4. Luminosity, L, was computed from:

$$L = \left[\frac{L}{I_1I_2}\right] \frac{1}{\tau} \int_{(I_1I_2)_{max}}^{(I_1I_2)_{min}} I_1I_2 dt$$

5. The $\int_{(I_1I_2)_{max}}^{(I_1I_2)_{min}} I_1I_2 dt$ and half life, τ, each have two entries. The entry under I applies for the first fifty-one phased runs. The entry under II applies for runs 52 through 70.

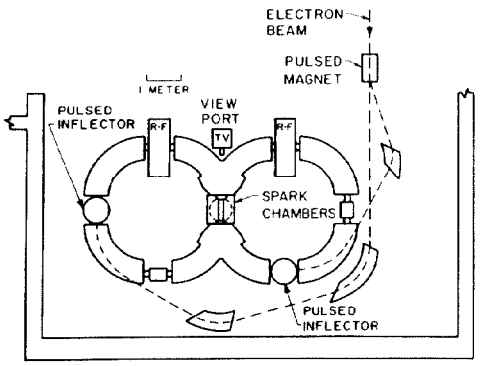

Fig. 1. Layout of Storage Ring.

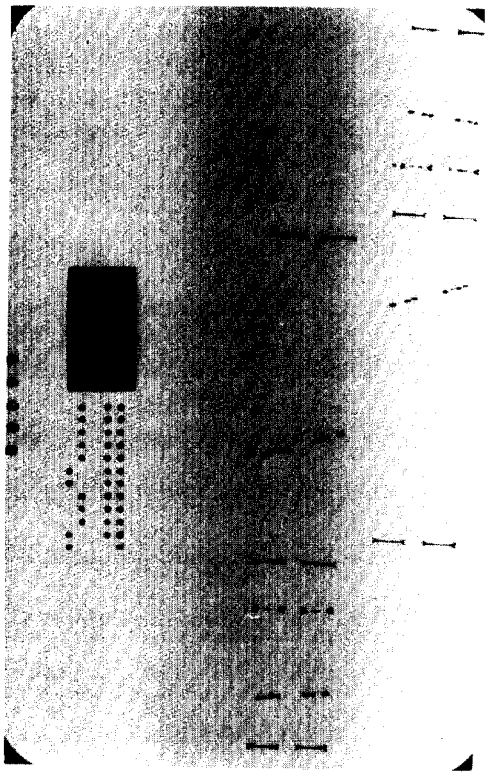

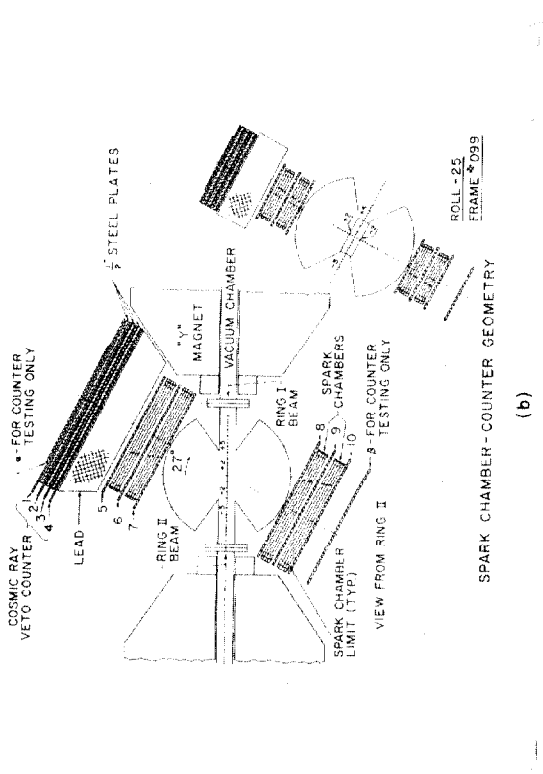

Fig. 3. Spark Chamber Picture and Reconstruction.

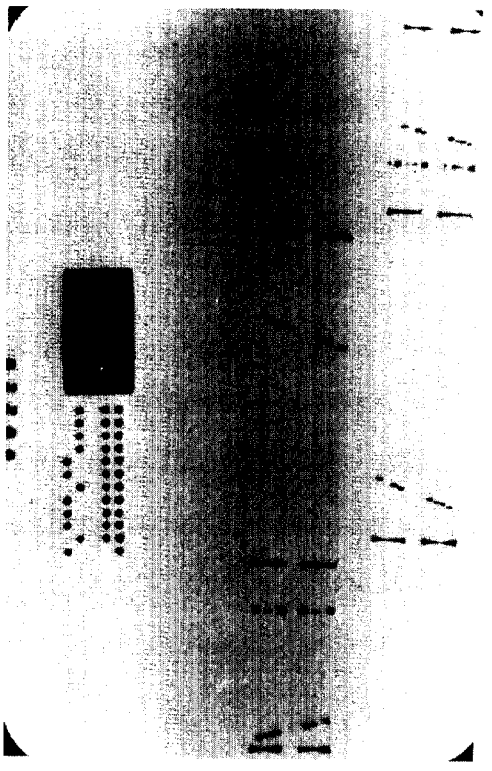

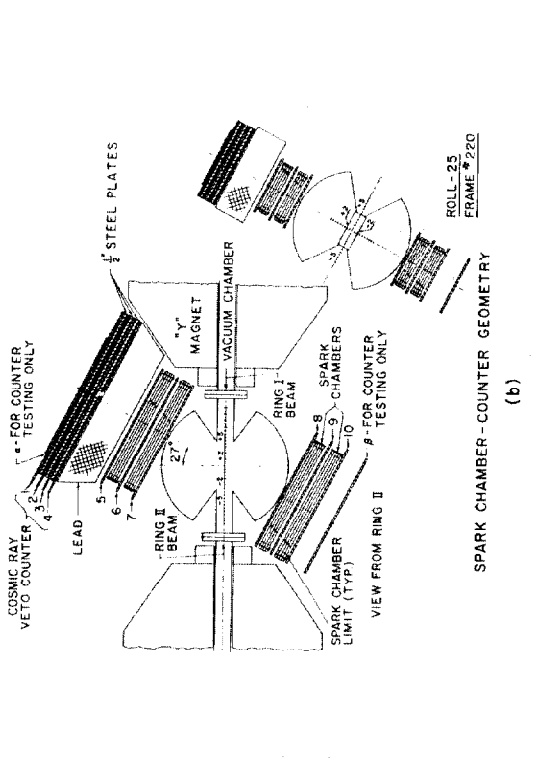

Fig. 2. Spark Chamber Picture and Reconstruction.

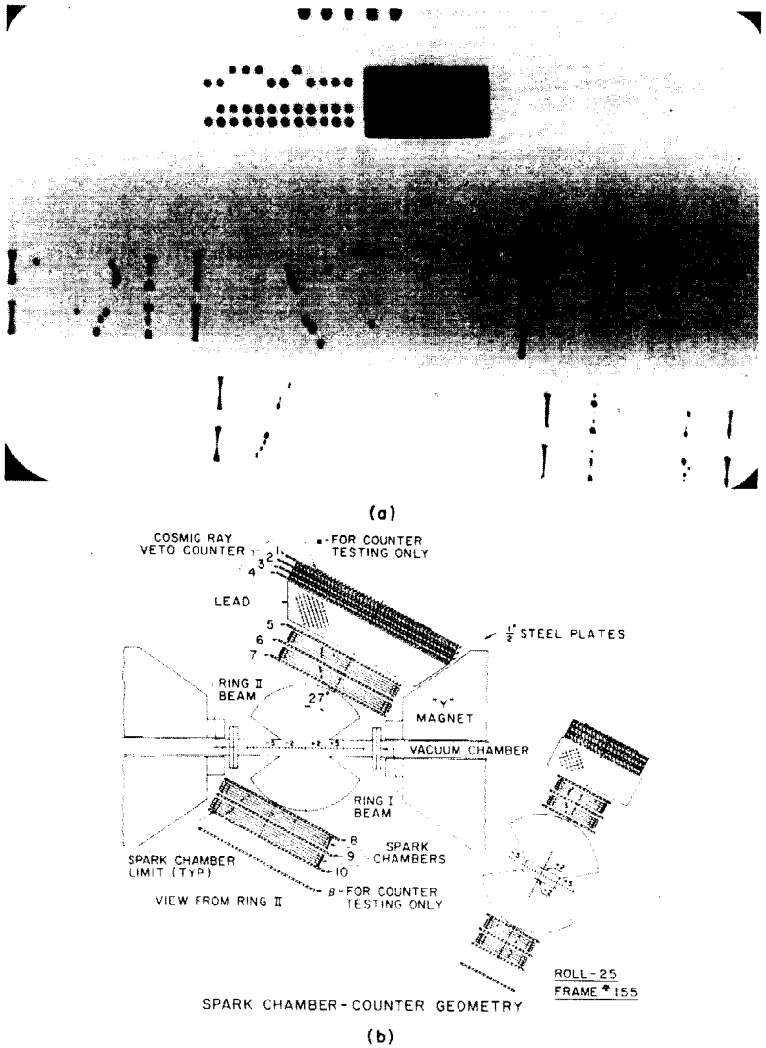

Fig. 4. Spark Chamber Picture and Reconstruction.

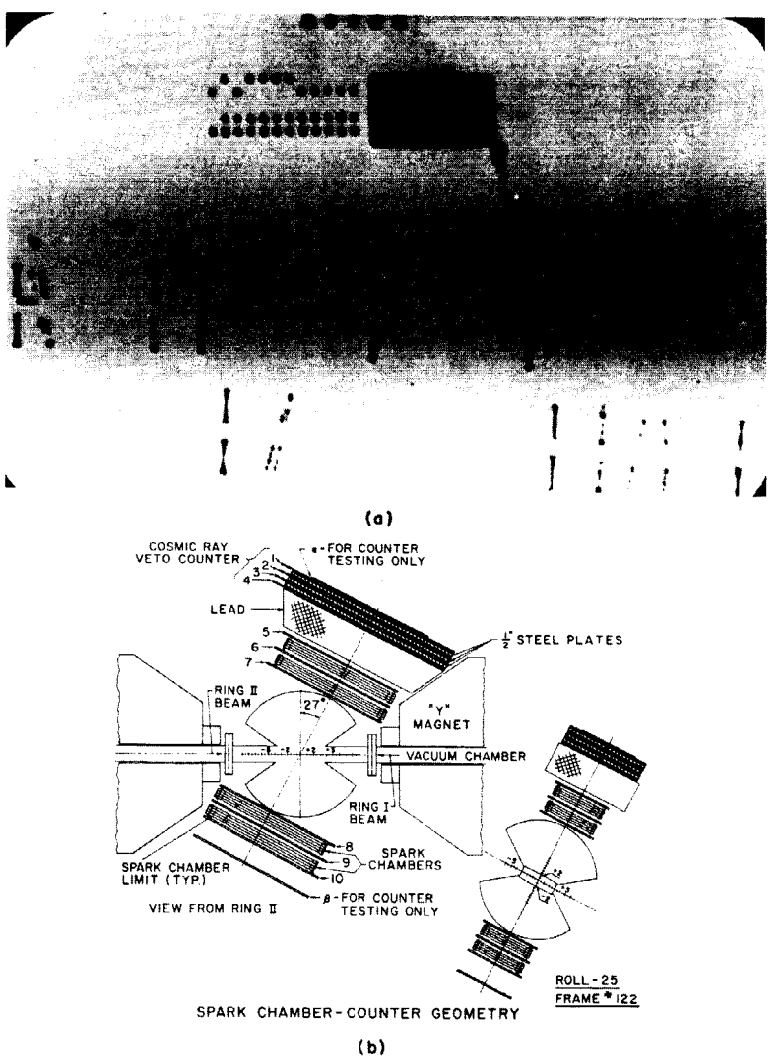

Fig. 5. Spark Chamber Picture and Reconstruction.

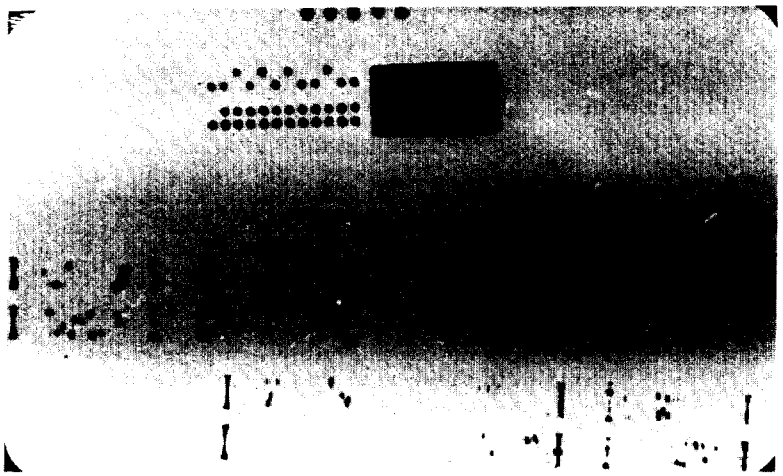

(a)

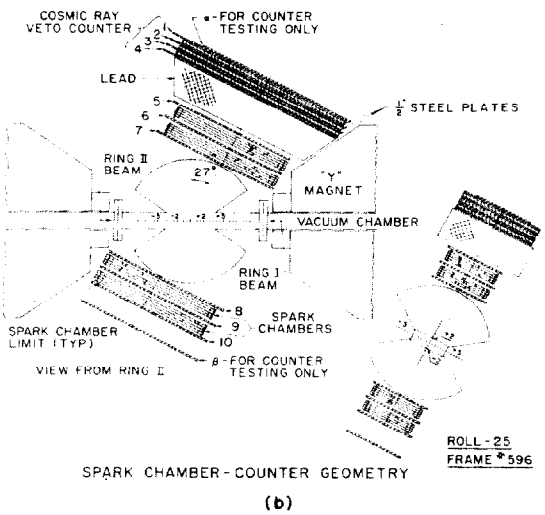

(b)

Fig. 6. Spark Chamber Picture and Reconstruction.

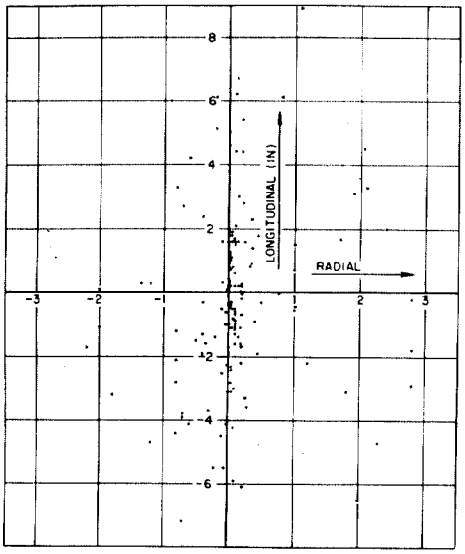

Fig. 7. Intersection of Track with Median Plane, All Collinear Events, Beams Phased (70 runs).

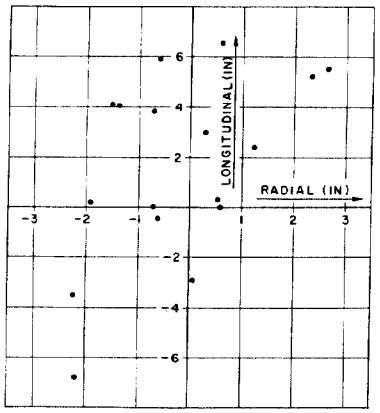

Fig. 8. Intersection of Track with Median Plane, All Collinear Events, Beams Dephased (22 runs).

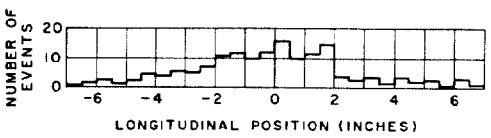

Fig. 9. Intersection of Track with Median Plane, Longitudinal Distribution (summed over all radial positions), Beams Phased.

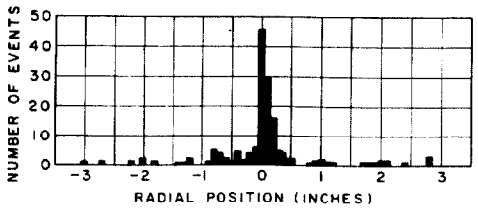

Fig. 10. Intersection of Track with Median Plane, Radial Distribution (summed over all longitudinal positions), Beams Phased.